Computational Materials Science 214 (2022) 111690

Contents lists available at ScienceDirect

Computational Materials Science

journal homepage: www.elsevier.com/locate/commatsci

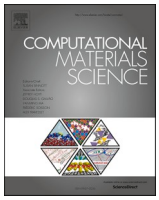

Full Length Article

# Temporal evolution of the behavior of absorbed moisture in a damaged polymer-quartz composite: A molecular dynamics study

Rishabh D. Guha [a], Farzin Rahmani [b], Katherine Berkowitz [a], Melissa Pasquinelli [b], Landon R. Grace [a,*]

[a] Department of Mechanical and Aerospace Engineering, North Carolina State University, Engineering Building-III, 911 Oval Drive, Raleigh, NC 27606, United States
[b] Department of Forest Biomaterials, College of Natural Resources, North Carolina State University, Biltmore Hall, 2820 Faucette Drive, Raleigh, NC 27606, United States

ARTICLE INFO

*Keywords:*
Composites
Fiber-matrix interface
Moisture
Debonding
Molecular dynamics

ABSTRACT

Exposure of a composite structure to mechanical or environmental stressors often leads to the formation of damage sites which contain rupture mechanisms such as matrix cracking and interfacial debonding. Continued accumulation of this type of small-scale damage can cause sudden and catastrophic large-scale failure. A novel damage characterization technique which leverages the altered physical and chemical states of naturally absorbed moisture in response to sub-micron scale damage has recently shown promise for early detection of damage. In this work, molecular dynamics simulations are used to better understand the differences in the behavior of absorbed water molecules near a damage site. The results show that, irrespective of the initial distribution of molecular water throughout the composite, or the presence of polar atoms in the polymer matrix, water tends to preferentially cluster near the damage location. It was also found that spatial confinement near the polymer-fiber interface hinders diffusion of the water molecules into the polymer matrix. These molecular level insights bolster the hypothesis formulated in previous experimental studies that absorbed moisture behaves like free water in terms of its dielectric activity when the water molecules agglomerate at the damage location. Consequently, this locally distinct permittivity can be leveraged for damage detection and quantification.

## 1. Introduction

The need for enhanced performance has propelled the use of epoxy-based polymer materials in different engineering sectors. They provide viable options as encapsulants in the microelectronic packaging industry [1] owing to their thermal stability [2,3] and resistance to chemical contamination [4]. Concurrently, there is an ever-increasing demand for epoxy composites as a structural component in the automotive and aerospace sectors [5] due to a high strength to weight ratio [6]. The glass/quartz reinforced epoxy composites also have a low dielectric constant [3] which leads to better electrical insulation properties [7]. Based on current predictions, the global composite market will be worth over 146 billion USD by 2026. However, unlike conventional materials like steel, polymer matrix composites (PMC) do not show any signs of early-stage damage from common low velocity impact events like hail strikes or tool drops [8]. It is also very difficult to identify damage initiation caused by cyclic thermal loads or track fatigue damage progression [9]. This complicates any efforts of long-term service life prediction and makes these components susceptible to sudden and catastrophic failure. Further exacerbating the problem, polymer composites are frequently subjected to fluctuating cycles of temperature and humidity [10] and have a propensity to absorb environmental moisture [5,6,11]. The absorbed water molecules degrade the overall properties of a composite as it leads to matrix plasticization, suppression of glass-transition temperature ($T_g$) [12], degradation of the fiber-matrix interface [13], moisture induced swelling [14] and associated generation of damage sites through microcracks [15].

Significant research has been performed to develop damage characterization techniques in polymer composites but none of the existing ones have excelled in accuracy, financial feasibility, or flexibility. Consequently, manual techniques like visual inspection and the 'tap test' are still widely used for evaluating composites despite the presence of sophisticated methods like ultrasound, thermography, x-ray computed tomography, shearography and acoustic emission monitoring to name a few [16–18]. The deleterious effects of moisture in composites has already been discussed but its ubiquitous nature, especially during

* Corresponding author.
*E-mail address:* lgrace2@ncsu.edu (L.R. Grace).

https://doi.org/10.1016/j.commatsci.2022.111690
Received 11 April 2022; Received in revised form 8 July 2022; Accepted 25 July 2022
Available online 5 August 2022

service life makes low levels of absorption practically unavoidable. The nature of the polymer-water interactions in a PMC is extremely complex, but a fundamental understanding of this behavior can serve as the cornerstone for developing a novel Non-Destructive Evaluation (NDE) technique as evidenced in these studies [11,19–24]. The behavior of water in a polymer network is primarily influenced by the secondary interactions it is involved in with its surrounding atoms, and the free volume available in the forms of nanopores and voids [25,26]. Molecular water is highly polar and as it ingresses into a polymer matrix, it engages in hydrogen-bonding and other weaker non-bonded interactions with the polar sites in the network. But the matrix is a highly crosslinked three-dimensional structure with available free volume where water molecules can potentially cluster together. The state of moisture in a polymer network has been investigated through various characterization techniques like infrared spectroscopy (FTIR), Nuclear Magnetic Resonance (NMR), and dielectric relaxation. Pethrick et al. [27] were able to successfully use dielectric relaxation to conclusively identify different states of water molecules in the network with distinct relaxation frequencies. These water molecules were identified as either "bound" to the network or "free" from any external secondary interactions residing in nanopores, microcracks and voids. The theory of this duality of water molecules in a polymer network was later bolstered by spectroscopic studies conducted in the medium and near infrared range (MIR and NIR) by Herrera-Gomez et al. [28] and Musto et al. [29–31]. Based on this duality of water molecules, Altan et al. developed a new non-Fickian diffusion model [32–34] for predicting moisture absorption in composites which accounts for the hindered diffusion due to physical or molecular interactions at the microscale.

The "free" and "bound" water molecules respond differently to applied electromagnetic fields since they have different polarization tendencies, which in turn is inextricably linked to relative permittivity. Within the microwave frequency range of 1–10 GHz "bound" water has a dielectric constant similar to ice, having a magnitude of ~3.2 [5,35]. In contrast, "free" water molecules exhibit a dielectric behavior similar to bulk water (relative permittivity ~80) across a wide range of frequencies (1.3–40000 MHz) [36]. The preferential migration of free water molecules to damage sites coupled with their distinctly different relative permittivity allows us to leverage moisture as a damage indicator for an in-service composite. This technique of detecting physical damage in moisture contaminated composites has already been established in previous experimental studies using dielectric resonance [11,19–22] and NIR spectroscopy [23,24] but a molecular level picture studying the behavior of absorbed water molecules in a damaged composite is still missing.

Molecular Dynamics (MD) simulations have been extensively used to study the properties of crosslinked polymer networks [37–39], the non-bonded interactions of these networks with small penetrant molecules (like water), and the eventual impact of moisture absorption on mechanical and thermal properties [40–42]. The secondary interactions between water and network sites have been quantified through hydrogen bond (H-bond) concentration and two different types (Type-I and Type-II) of H-bonds have also been identified [43–45]. The Type-II water molecules exhibit similar properties as 'bound' water and are engaged in extensive secondary bonding with the polymer. They contribute towards lowering the relative permittivity of the absorbed water molecules while Type-I water molecules cluster in the available free volume in the network and exhibit a higher dielectric constant [45,46]. But these previous studies have only analyzed systems which differ in chemical morphology or network topology (crosslinking density). They do not include the effects of additional free volume created by damage or behavioral changes of the absorbed water molecules at the fiber-matrix interface when a fiber reinforcement is introduced in the system. The interface has been previously analyzed using MD simulations and multiple studies have discussed the reduced interfacial adhesion due to moisture ingress [13,47–52]. A recent study by Walsh et al. investigated the mechanism of moisture transport at the interface and the network in a carbon fiber reinforced composite subjected to hygroscopic aging. [53].

This work attempts to use MD for simulating the behavior of water molecules in an epoxy-quartz composite with increasing degree of damage. The damage was modelled in the form of interfacial debonding, which is a common mode of early-stage damage involving both the fiber and the matrix. The temporal evolution of the water molecules was analyzed to understand the impact of the initial concentration profile of absorbed moisture on the eventual distribution in the composite, especially near the damage site. The interaction behavior between different units of the composite (fiber, matrix, and sizing) was also investigated to understand how water molecules influence the non-bonded atomic interactions across the composite. Implications of increasing extent of damage on the mobility of the water molecules was also studied. The outcomes of this study allow us to better explain the localized rise of relative permittivity in in-service damaged composites and provide a nanoscale snapshot of the molecular interactions driving the newly developed moisture assisted NDE technique [21,22].

## 2. Simulation details

The open-source software package, LAMMPS [54] was employed for all molecular dynamics (MD) simulations in this study. All the molecular models were constructed using the Amorphous Builder module in the commercially available MAPS platform of Scienomics (Materials and Processes Simulations Platform, Version 4.2.0, Scienomics SARL, Paris, France). The SciPCFF forcefield was assigned to describe the bonded and non-bonded interactions between individual atoms [55]. This forcefield is a MAPS implementation of the class-II polymer consistent force field (PCFF). For the bonded molecular interactions, SciPCFF borrows its equations from PCFF while it uses bond increment parameters of various compounds from the COMPASS force field for the assignment of atomic partial charges [56,57]. The particle-particle particle-mesh (PPPM) solver was used with a tolerance of 1E-4 for the long-range interactions and the cutoff for the non-bonded interactions was set at 12 Å for both the van der Waals and the electrostatic forces.

The composite system modelled in this work comprises of three different units- the quartz fiber, the sizing, and the epoxy matrix respectively. The sizing is a chemical component which is coated on the fiber reinforcement. It serves as a coupling agent between the fiber and the matrix enhancing the overall interfacial adhesion between the two components. The silane coupling agent $\gamma$-Aminopropyltriethoxysilane (AMPTES) which has been previously used in molecular modelling of glass-epoxy composites [58,59] was selected as the sizing. The epoxy-hardener combination Diglycidyl Ether of Bisphenol A (DGEBA) and Diethylene Tetra Amine (DETA) was used to model the epoxy matrix. This combination is frequently used in composite matrices and its properties have been extensively studied through simulations and experiments. The molecular models for the sizing, epoxy and hardener have been shown in the SI in Figure S1 (a), (b) and (c) respectively. The choice of the epoxy and hardener was also consistent with our previous simulation studies [43–45] which explored the molecular interactions of absorbed moisture in the composite matrix. A typical quartz fiber has a diameter of around 10 μm which can be approximated as a flat slab in our nanoscale model (dimensions in Å). A (1 0 0) crystal plane of quartz was chosen as the unit cell and replicated fifty times to construct the quartz fiber. Thirty-six molecules of AMPTES were randomly grafted on the surface of the quartz slab without any overlapping. These grafted molecules represent a sizing coating adhesively bonded on the fiber. For this epoxy-hardener combination, crosslinking occurs through the formation of covalent bonds between the $-CH_2^+-$ site in the epoxy and the $-N_2^-$ site in the hardener. In our earlier works, the crosslink between reactive epoxy-hardener sites was performed dynamically using a Python script. But as discussed by Yu et al. [60], this technique becomes complex when the system size becomes large. In this study, the representative molecule method (RMM) was used to generate the crosslinked

systems. RMM creates a representative unit for a crosslinked epoxy and then packs multiple units in an amorphous simulation cell. Results have shown that besides being simpler, this method also produces results which are closer to experimental data [48,61]. Crosslink bonds were created between eight molecules of the hardener and sixteen molecules of the epoxy which served as the representative molecule. The 1:2 ratio was maintained because each molecule of the hardener is tetrafunctional and is capable of executing four crosslinking reactions, compared to the hardener which is bifunctional. The epoxy ring was closed for the unreacted $-CH_2^+-$ groups in this crosslinked chain and the hydrogens were adjusted in the unreacted $-N_2^-$ sites to prevent any valency violation. A molecular representation of one of these crosslinked units has been shown in Figure S2; eight such chains were packed on top of the quartz-sizing to construct a quartz fiber composite. Since we are trying to model damage resulting from debonding, the extent of damage was varied by creating different models with increasing interfacial gaps between the quartz-sizing and the matrix. The reference was an undamaged model without an externally enforced interfacial gap between the matrix and the fiber while three damaged scenarios were simulated by introducing interfacial gaps of 2, 4 and 6 Å respectively. These narrow gaps are molecular level representations of debonding in the damage initiation phase when it is particularly difficult to detect. Fig. 1 (a, b, and c) compares the increasing degree of interfacial debond in the damaged models.

The simulation cells for all the four models consisted of 10,884 atoms. Each of the models had 128 molecules of DGEBA crosslinked with 64 molecules of DETA and an average overall crosslinking of ~81%. The simulation workflow followed for the dry damaged and undamaged models borrow its methodology from our previous works [43–45] and the details of the workflow has been added in Section 3 in the SI. For the reference model, the water molecules were dispersed in the epoxy matrix. In case of the damaged models, two different initial states were studied. For the first scenario, all water molecules were concentrated at the damage interface as seen in Fig. 2 (a) and in the second case, the water molecules were dispersed in the epoxy matrix (Fig. 2 (b)). These two different scenarios of initial moisture distribution was adopted earlier by Cho et al. [62] to study the interfacial traction in a graphene oxide-epoxy nanocomposite. In this work, the two cases enabled us to observe the difference in temporal behavior of the water molecules when they are concentrated near the damage area compared to being dispersed throughout the polymer network. Three representative models were created for each model type (1 undamaged and 3 damaged) by randomly perturbing the initial positions of the water molecules in the system. As a result, we obtained 21 different simulation systems: 4 model types with 2 different initial distributions for absorbed moisture.

Table 1 gives a summary of the different types of composites models and the simulation scenarios based on the initial position of water molecules. The multiple systems allowed us to calculate an average value for any property and reduce the probability of any outlier. Subsequently the models were subjected to a 500-step geometry optimization process using the Steepest Descent method. For the simulations after moisture introduction, the models were represented as semi-infinite.

The PBC was enforced in only the x and y direction, since enforcing the PBC in 3 dimensions would allow the water molecules near the fiber to interact with the epoxy network of the replicated simulation cells in the z-direction. We used a non-periodic boundary condition with a fixed boundary in the z-direction. A vacuum of 10 Å was applied on top of the polymer matrix and the reflective wall condition was imposed on the fixed boundary to prevent any atoms from moving out of the simulation box. Post-optimization, a long production run of 20 ns (20000 ps) was performed for both the undamaged and the damaged simulation cells using the NVT ensemble. The temperature was fixed at 300 K and the Nose-Hoover thermostat was applied with a damping coefficient of 10 fs. A sufficiently long production run was necessary to understand the behavior of the absorbed moisture as it interacted with the polar sites in the polymer network and the localized free volume created due to the fiber-matrix debonding (interfacial gap).

The systems were then analyzed at two different points in the simulation trajectory:-.

(i) In the beginning of the production run at 1 ns
(ii) At the end of the production run at 20 ns

A quantitative comparison of the properties at these two temporal state points across the different models allowed us to understand the evolving behavior of the water molecules, especially near the damage site.

## 3. Results and discussion

### 3.1. Density profile

The preferential residence sites for the ingressed water molecules in the models was investigated by comparing the density profile (molecules/Å$^3$) along the z-axis. The variation in the profile with simulation time allowed us to capture the behavior of the water molecules near the damaged.

interface. From the molecular model in Fig. 2, it was calculated that the quartz slab starts at ~8 Å along the z-axis with a thickness of ~8 Å. We can see a very small peak at that z-position for all the models. This

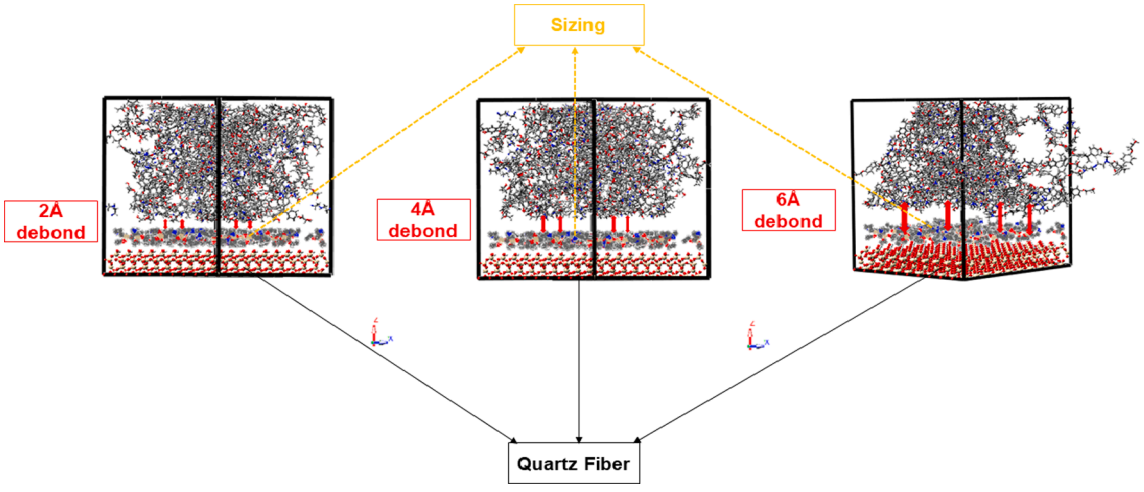


**Fig. 1.** Molecular models showing the increasing degree of interfacial damage in (a) 2 Å debond (b.) 4 Å debond and (c) 6 Å debond.

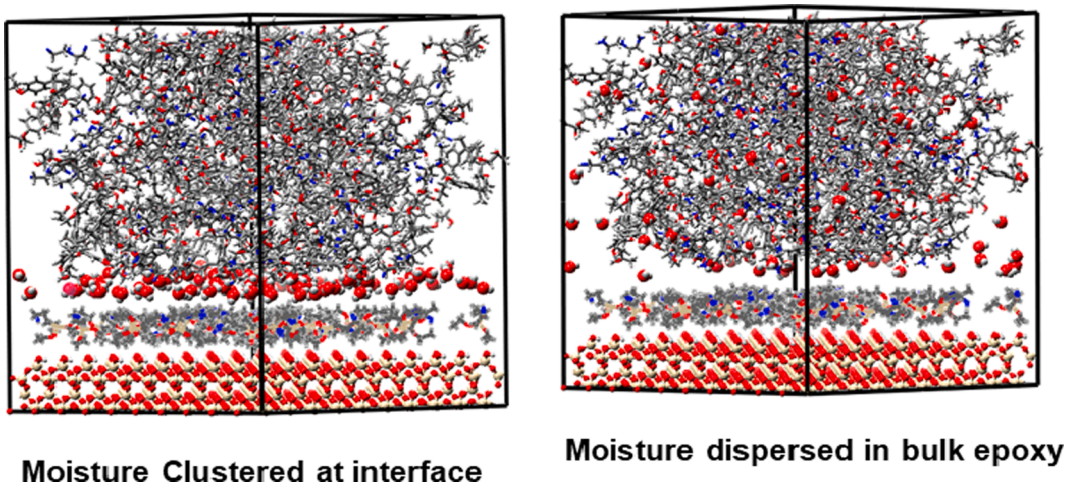


**Fig. 2.** Two scenarios of initial moisture distribution in the damaged models. (a) Moisture clustered at the damage interface and (b) Moisture dispersed in the polymer epoxy.

**Table 1**
Summary of the moisture contaminated damaged composite models.

| Model Type | Scenario 1: Moisture concentrated at interface | Scenario 2: Moisture dispersed in polymer matrix |
|---|---|---|
| Undamaged Reference (No externally enforced interfacial debond) | N/A | 3 representative models |
| 2 Å interfacial debond | 3 representative models | 3 representative models |
| 4 Å interfacial debond | 3 representative models | 3 representative models |
| 6 Å interfacial debond | 3 representative models | 3 representative models |

indicates that although an external interfacial gap was not enforced between the sizing molecules and the quartz, a very small fraction of water molecules can potentially diffuse at the sizing-fiber interface. Fig. 3(a) serves as the undamaged reference and we can observe that the density profile in this model does not change appreciably with time. A minute peak can be observed near the sizing-epoxy interface which indicates that the water molecules initially tend to travel towards the discontinuity in the model but due to the lack of a localized free volume, very few of them can accumulate and the rest of the moisture gets uniformly dispersed in the polymer matrix. Consequently, when we look into the profiles for the damaged models, we can observe a couple of things. As expected, when the water molecules are initially concentrated at the fiber-matrix debond, a higher number of water molecules remain clustered at the damage site at 1 ns. But, since the concentration of moisture is the same across models while the damage volume varies, we can see that in the 2 Å debond model, the water molecules start diffusing out and we observe a broad shoulder in the polymer bulk close to the damage site. When we compare this to the 1 ns density profile for the 4 Å and 6 Å models with larger damage volumes, the water molecules stay localized near the fiber-matrix debond and do not diffuse out as quickly as the 2 Å model. As a result, we get much sharper and broader peaks indicating greater residence times for the water molecules in the damage site and slower diffusion out into the network. On the other hand, when the water molecules are dispersed in the polymer bulk, they diffuse towards the damage site as the simulation time progresses. When only 1 ns of the simulation time is complete, we can see that there is no indication of clustering at the damage site especially in the models with greater degree of damage (4 Å and 6 Å debond). In case of the undamaged and 2 Å debond model, there is no obvious clustering near the damage site at 1 ns when the water molecules are dispersed in the network, but a greater concentration of moisture diffuses towards the fiber-matrix interface. The quicker transport of the water molecules might be attributed to the Coulombic attraction forces between the sizing and the polymer network which have a smaller separation distance in case of these two models. As the simulation time progresses to 20 ns and the water molecules navigate the entire model, we can see that the density profile in the damaged models start to converge irrespective of the initial position of the molecules. Although in one scenario moisture diffuses out of the damage site and into the network and, in the other one, they diffuse into the damage site from the bulk, they eventually cluster near the interface and the equilibrium profile is very similar irrespective of the initial position of the water molecules in the models. The final density near the damage site is dependent on the interfacial gap and that can be observed in the peak areas near the damage volume as seen in Fig. 3 (b), (c) and (d). The secondary peaks at the end of the damage interface in all models reaffirm the hypothesis that the water molecules tend to cluster near the debond site, especially when the damage volume is not large enough to accommodate all the water molecules. The peak heights and width increase with the fiber-matrix interfacial gap and the average number of water molecules residing in the damage site can be calculated by integrating the density profile as seen in Table 2. The results in Table 2 follow the expected trend of a greater degree of accumulation with an increase in damage volume. The average number of water molecules at the damage site at the end of the simulation is always higher when the water molecules are initially concentrated near the interface. This is probably due to a combination of higher initial concentration and a slower moisture diffusion rate out into the polymer matrix from the damaged region.

### 3.2. Radial distribution functions

As discussed in our previous studies, the Radial Distribution Function (RDF) is defined by the probability of finding a particle at a distance "r" from a given reference particle and in case of a polar system like a moisture-contaminated quartz-composite model, it can serve as a qualitative tool to determine the probabilistic distribution of non-bonded hydrogen bonds (H-bonds) between two polar species. In this study, the non-bonded interactions will depend not only on the partial charges of the polar sites but also on the relative location of the water molecules with respect to the damaged composite. The RDF will also vary depending on when it is calculated on the temporal scale of 0 to 20 ns. In this study, we have considered two different RDFs to account for the different interactions a water molecule can engage in within the composite network. The intermolecular RDF between the hydrogen and the oxygen atoms of the water molecules (Ow-Hw) was calculated and then we proceeded to calculate the RDF between the oxygen atoms in the

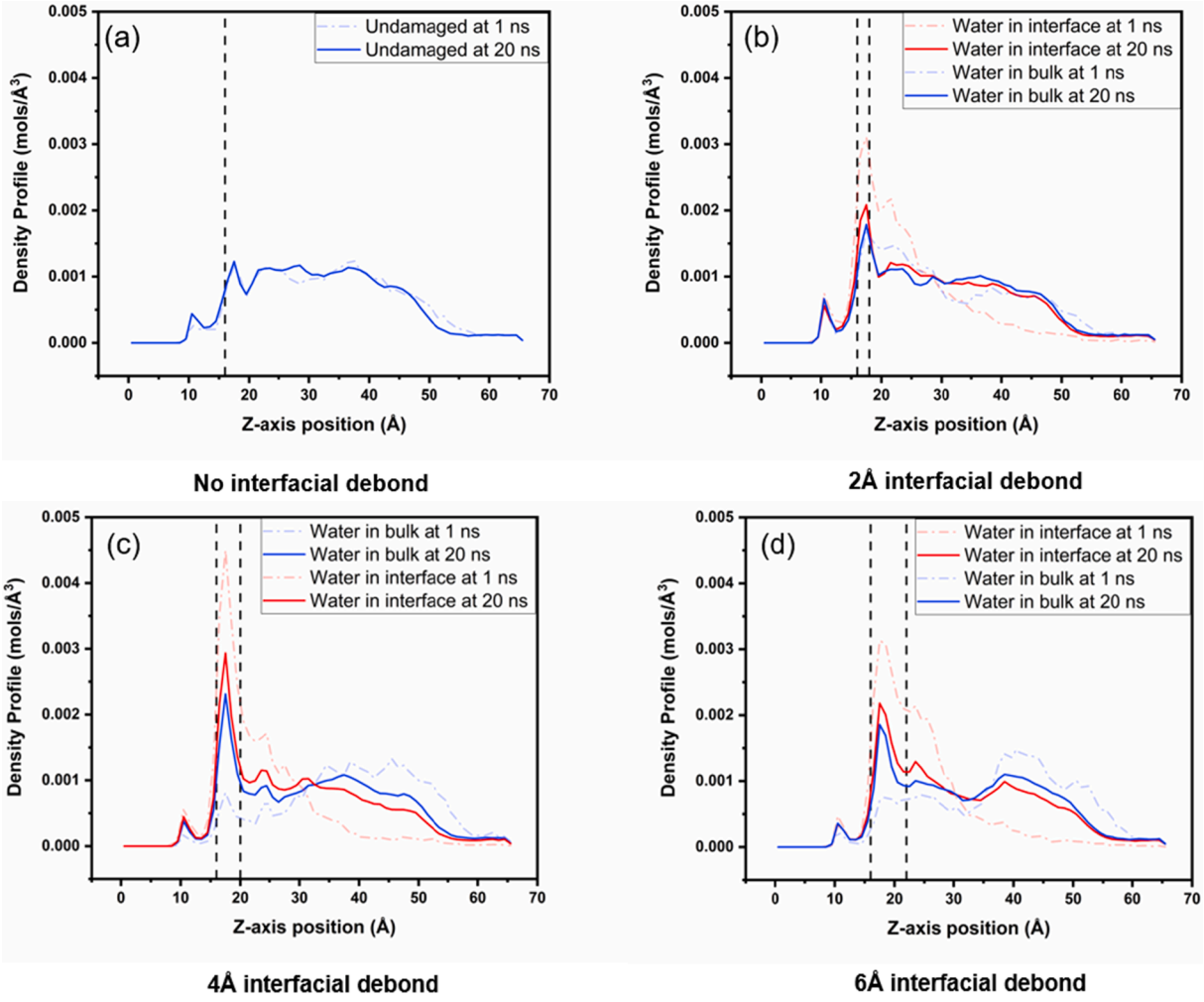


**Fig. 3.** Average density profile for the water molecules along the z-axis at (i) 1 ns and (ii) 20 ns. The black dotted lines indicate the beginning and end of the damaged interface in the models.

**Table 2**
Average number of water molecules near the damaged interface at (i) 1 ns and (ii) 20 ns.

| Type of model | Water initially concentrated at interface | | Water initially dispersed in polymer | |
|---|---|---|---|---|
| | 1 ns | 20 ns | 1 ns | 20 ns |
| 2 Å interfacial debond | 22.48 | 14.23 | 12.01 | 12.22 |
| 4 Å interfacial debond | 42.08 | 25.27 | 7.42 | 19.83 |
| 6 Å interfacial debond | 46.94 | 28.07 | 12.55 | 22.69 |

water molecules and the oxygen atoms in the polar hydroxyl sites present in the crosslinked network (Ow-OH). The mutual interactions of the water molecules in the composite can be explained by the Ow-Hw RDF, while the Ow-OH RDF helps us understand the interactions of the host network with the penetrant molecules, i.e. water. In the Ow-Hw RDF plots (Fig. 4 (a) and (b)), we observe two clear peaks at ~1.9 Å and ~3.2 Å. As discussed in previous investigations of intermolecular RDF, the peaks within 3.5 Å are due to H-bonding while any peaks beyond that are due to the effects of weaker secondary interactions like van der Waals and electrostatic forces [63,64]. The H-bonding between water molecules manifests in the RDF as the two peaks with the second peak representing the H-bond between the oxygen and the second hydrogen of the interacting water molecules [65,66]. Fig. 4 compares the intermolecular Ow-Hw interactions for the 6 Å debond damaged composite at 1 ns and 20 ns respectively. Similar comparative graphs for the 2 Å debond and the 4 Å debond models have been included in Figures S4-I-IV in the SI. In Fig. 4 (a), we can see that initially when the water molecules are concentrated at the damage site (scenario 1), they have a much higher probability of forming an intermolecular H-bond with another water molecule. This can be seen in the significantly higher RDF peaks when 1 ns of the simulation is complete. But as the simulation progresses, the water molecules disperse out and navigate the polymer network. Consequently, they also start forming H-bonds with the polar sites in the epoxy and the RDF peaks dip to lower magnitudes at the end of the simulation. This shows that in the beginning of the simulation the water molecules have a higher tendency to associate with other water molecules due to the presence of the cluster near the damage site. On the other hand, when the water molecules are dispersed in the epoxy (Fig. 4 (b)), the peak heights do not change appreciably and there is not a significant difference between the damaged and the undamaged RDFs throughout the simulation time period. This is an artefact of the extensive non-bonded interactions between the epoxy and the water molecules from the beginning of the simulation. In line with the results of the density profile, the RDF peak magnitudes at the end of the simulation for both damaged scenarios converge to very similar values.

The intermolecular RDF between moisture and the polar sites in the composite matrix (Ow-OH) has been compared in Fig. 5 ((a) and (b)). The sharp peak at ~2.8 Å in these plots corresponds to the H-bond length between a hydroxyl site and a water molecule. For this interaction, we can observe a reverse trend when we compare the peak with the previous RDF for interacting water molecules (Fig. 4). Initially, when the

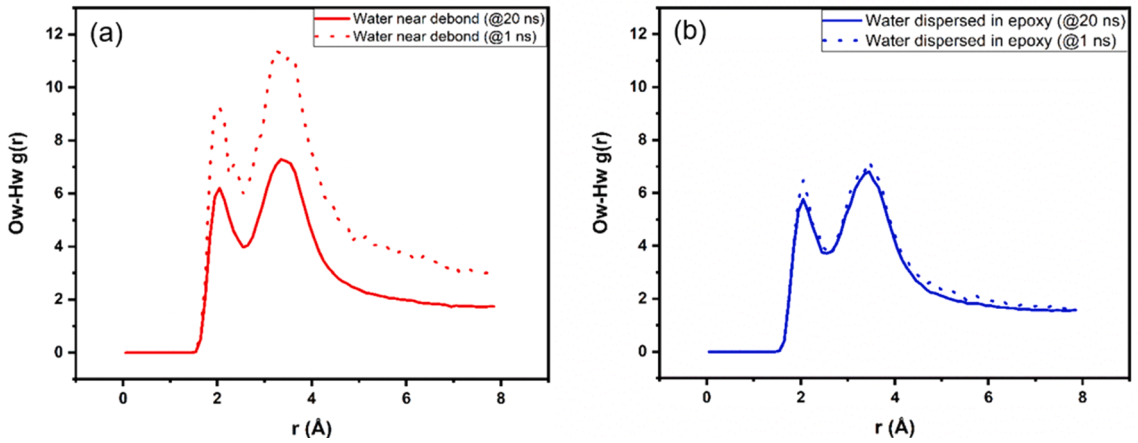


**Fig. 4.** Ow-Hw RDF for a damaged model at (i) 1 ns and (ii) 20 ns when (a.) water is concentrated near debond and (b.) water is dispersed in epoxy.

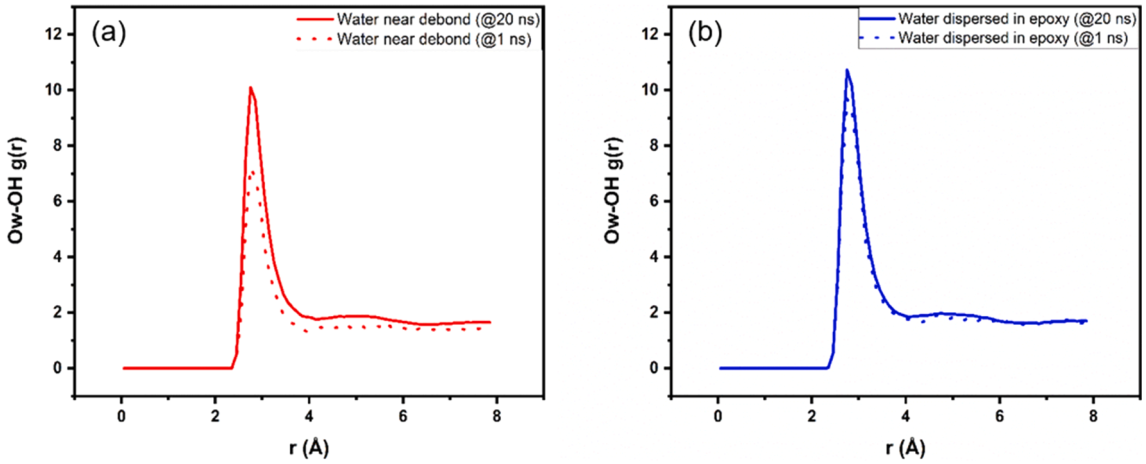


**Fig. 5.** Ow-OH RDF for a damaged model at (i) 1 ns and (ii) 20 ns when (a.) water is concentrated near debond and (b.) water is dispersed in epoxy.

water is concentrated at the damage interface (Fig. 5(a)), the non-bonded interactions are dominated by the H-bonds formed between water molecules. As a result, when we look at the Ow-OH RDF at 1 ns, we observe that the peak is appreciably low. As the simulation proceeds, the water molecules diffuse into the network and start interacting with the polar sites. Consequently, the same RDF peak at 20 ns is much higher than at 1 ns, which is a clear indication of the higher H-bonding activity of the water molecules with the network over time. Similar to the Ow-Hw RDF, the Ow-OH RDF peak in Fig. 5(b) does not show much variation when the water molecules are initially dispersed in the epoxy network. The peak is in fact slightly lower at 1 ns when the water molecules are dispersed in the polymer. This slight dip is likely because moisture has not interacted with all of the possible polar sites at the beginning of the simulation.

Another interesting artefact is observed when the final RDF peaks at 20 ns are compared for the three damaged models. As seen in Fig. 6(a, b and c), when the damage interface is narrow, i.e. 2 Å, the Ow-Hw RDF peaks practically superimpose on each other indicating no difference in

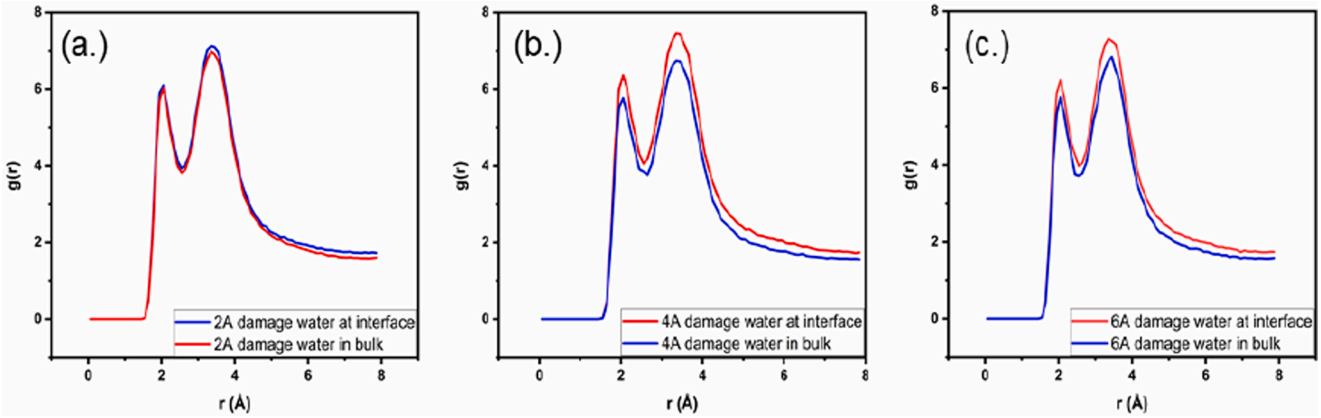


**Fig. 6.** Ow-Hw RDF peak at the end of the simulation for both the damage scenarios for a.) 2 Å debond b.) 4 Å debond and c.) 6 Å debond.

final H-bonding activity for both the initial scenarios of moisture distribution. But as the damage interface becomes wider, the final RDF peaks are slightly higher for scenario 1. This is a result of the higher number of water molecules clustered at the damage site at the end of the simulation if they are initially concentrated at the interface for models with a greater degree of damage. It is consistent with the calculated values in Table 2, where we did not observe a significant difference in the number of water molecules near the damage site for the 2 Å debond model when compared to the 4 Å and 6 Å debond model. Similar results for the variation of the Ow-OH RDF have been compiled in Figure S5 of the SI. As expected, they show a reversal in peak heights and the Ow-OH peak is slightly higher for the damaged models for scenario 2 signifying the greater degree of interactions between the matrix and the absorbed moisture.

### 3.3. Interaction energy

The non-bonded energies between different units in the model can help us understand the role of damage in altering the molecular level interactions. The moisture-contaminated composite system is composed of 4 different entities- the quartz slab, the sizing molecules, the polymer epoxy network and the penetrant water molecules. The non-bonded interactions between these different units will evolve differently depending on the degree of damage and they were calculated through a separate set of 2 ns NVT simulations at 300 K. For instance, the interaction energy between the sizing molecules and the epoxy network will decrease as the separation between them increases at higher debond widths. This can be clearly seen in Figure S6, where the attractive interaction energy in the 2 Å debond case is consistently higher when compared to the other damaged models. The attractive interaction energies sequentially decrease as the sizing and the network gets further separated at increasing damage levels. A subtler difference in Figure S6 can be observed in the 2 Å debond case when the moisture is concentrated at the interface (damage scenario 1) compared to being dispersed in the bulk (damage scenario 2). When the water molecules are initially at the damage site, they form a molecular barrier between the network and the sizing, which marginally decreases the interaction energy between these two units at the beginning of the simulation. As the simulation progresses for the two different initial scenarios, the water molecules get equilibrated in the system and the interaction energies between the sizing and the network begin to converge.

The water molecules will also interact with the different units of the composite and its interactions will be stronger with the sizing molecules when they are near the damage site. These interactions have been summarized in Fig. 7 ((a), (b) and (c)) for the 2 Å, 4 Å and 6 Å debond respectively. Consistent with the results of the density profile, we can see in Fig. 7(a) that in case of the 2 Å debond model, when the water molecules are dispersed in the network, they quickly diffuse to the damage site and start interacting with the sizing molecules. This leads to an increase in attractive interaction energies as the simulation progresses. Conversely, when the water molecules are concentrated at the interface, there is a strong interaction at the beginning of the simulation, which decreases as the water molecules start diffusing out into the network. This trend is similar in all the three models but when the damage is low (2 Å debond), the energies converge quickly (before 1 ns) while in the other two damaged models, the convergence is slower. These interactions and their convergence align with our previous results for the density profile. In the case of the 2 Å model, when the water was dispersed in the bulk, the accumulation at the interface had started at 1 ns which is reflected here by the increase in attraction energy between the sizing and the water molecules. In comparison, the interaction energies are very low for the 4 and the 6 Å debond model when the water is dispersed in the polymer which reflects in the lower concentration of water molecules near the damage interface at 1 ns.

### 3.4. H-bonds

The multiple polar sites in the damaged composite will have partial charges due to their electronegativity differences. Additionally, water itself is a highly polar molecule with large electronegativity differences between the hydrogen and the oxygen atoms. The partial charges assigned to the polar atoms in this model have been tabulated in Table S1 in the SI. As mentioned earlier, the non-bonded polar sites in the model will interact with each other through the formation of H-bonds and the relative quantities of the different types of these bonds can help us in quantifying the preferential state of a water molecule in a damaged composite system. For this study, we have calculated a temporal average of the H-bonds at two different simulation states. The average H-bond quantity has been calculated from the first 1 ns of the simulation trajectory in the damaged systems, and then compared with the last 1 ns of the 20 ns trajectory. The last 1 ns of the undamaged system serves as the reference state for understanding how the water molecules are expected to behave in a pristine composite. In line with our previous studies, the H-bond was calculated using a Python script based on a geometric criterion, i.e., if the distance and the angle between a donor (partially charged positive site)-acceptor (partially charged negative site) was found to be below a threshold, then the H-bond quantity was incremented. The distance cutoff was 2.5 Å and the angle cutoff was 90°. A random water molecule in the composite model can form three different types of H-bonds.

(i) It can form an H-bond with another water molecule.
(ii) It can form an H-bond with the polar sites in the epoxy network

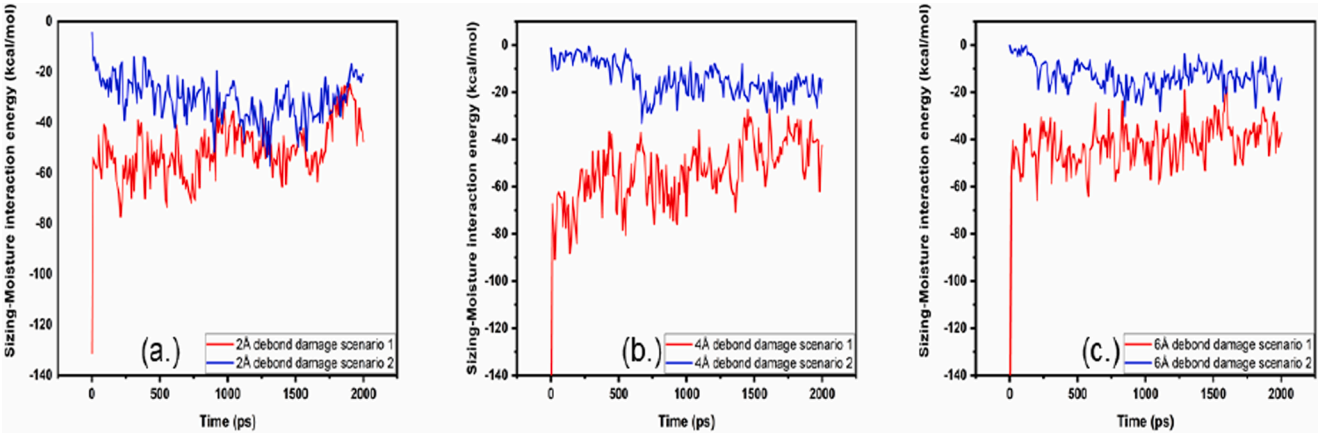


**Fig. 7.** Evolution of non-bonded interaction energy between the sizing molecules and absorbed moisture in a.) 2 Å debond b.) 4 Å debond and c.) 6 Å debond.

(iii) It can form an H-bond with the polar sites in the quartz fiber and the sizing molecules.

In our previous works which have analyzed the molecular interactions in a composite matrix, (i) and (ii) have been denoted as Type-I and Type-II bonds respectively. We have followed the same notation in this work and extended it by denoting (iii) as a Type-III H-bond. The H-bonding activity of the absorbed moisture for the three damaged models has been depicted in Fig. 8 and they have been normalized by the total number of bonds formed by the water molecules. The dotted reference lines indicate the normalized H-bond concentrations in the undamaged reference model. The results therefore show the probability of a water molecule to form a particular type of H-bond. The first thing we can observe is that in all the models, water has the highest tendency to bind to the network and form a Type-II H-bond. Conversely, the Type-III H-bond has the lowest probability of formation, even in the presence of damage. This is consistent with previous experimental studies, which have shown that moisture absorption in composites is primarily dominated by diffusion into the matrix while the fibers absorb negligible moisture [67]. If we look at the results from the first 1 ns when the water molecules are concentrated at the damage interface in all the 3 models, we observe that the water molecules have an appreciably higher tendency to form a Type-I H-bond while the Type-II H-bond formation probability is significantly lower than the undamaged reference. Interestingly, this is consistent with the RDF results of Section 3.2. The Ow-Hw RDF peak provides a qualitative probability of finding a water molecule at a distance which is consistent with the H-bond length. This probability is quantitatively vindicated by the Type-I H-bond formation tendency, which is higher when the water molecules are clustered at the interface. Similarly, the OH-Ow RDF peak is the reflection of the non-bonded interaction between water and the polar sites in the network and the lower OH-Ow RDF peak at 1 ns is due to the reduced probability of the water molecules to form a Type-II H-bond when they are near the damage site. We also observe that the Type-III H-bond formation probability is slightly higher in the initial phase of the simulation when the water molecules are concentrated at the interface (Scenario 1 first 1 ns). But as the simulation progresses, the water molecules diffuse out into the network and the Type-I and Type-II H-bonds start to match up with the reference undamaged system. At the end of 20 ns, regardless of the initial state of water molecules in the damaged system, the normalized H-bond concentrations are pretty similar with the damage systems having a slightly higher normalized concentration of Type-I or Type-III H-bonds and a lower concentration of Type-II H-bonds. These results match up with our observations in Sections 3.1 and 3.2. In section 3.1, we have already seen that there is an accumulation of the water molecules at the damage site which is independent of the initial state of moisture in the damaged systems. This clustering of moisture will increase the probability of water molecules to either engage in Type-I H-bonds with other water molecules at the damage site or engage in a Type-III H-bond with the sizing and the fiber. Additionally, if the final concentration at the end of the simulation is checked for the two damage scenarios in any of the 3 models, then we find that the Type-I concentration is slightly higher for damage scenario 1 with the Type-II concentration being lower. This comparison is depicted in Figure S7 and validates our previous results which have shown marginally greater moisture accumulation near the damage site when the water molecules are concentrated at the interface.

### 3.5. MSD and diffusion coefficient

The presence of damage in a composite influences its moisture absorption properties. Previous experimental studies have shown that absorbed moisture preferentially migrates to the micro-cracks and voids generated by damage events like low energy impact [11,19,21,22]. These damage sites act as cavities for the water molecules to cluster together away from the polar sites in the matrix and exhibit elevated

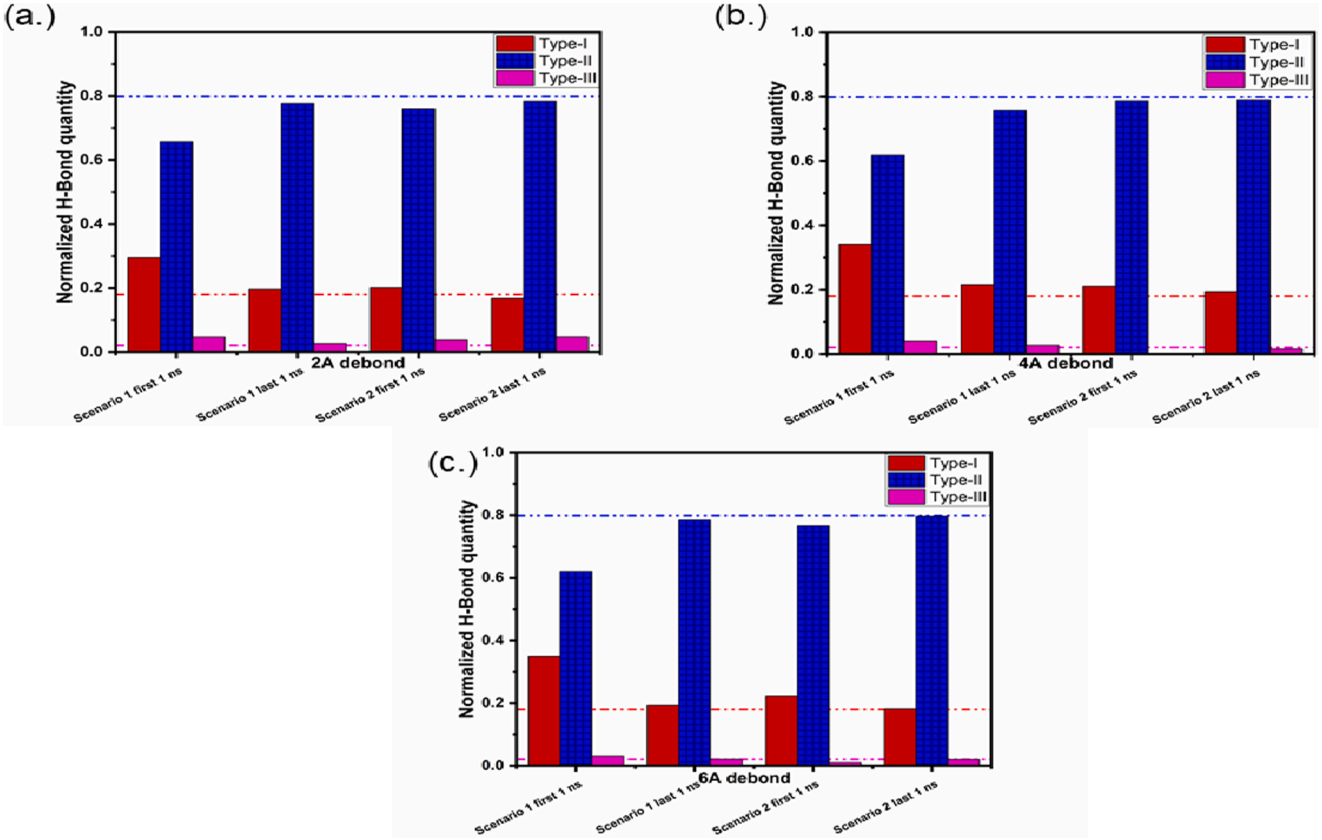


**Fig. 8.** Normalized H-bond concentration for absorbed moisture in a.) 2 Å debond b.) 4 Å debond and c.) 6 Å debond models.

dielectric signatures. This localized rise in dielectric constant can be used for sub-nanoscale damage detection and quantification.

In the polymer matrix, individual water molecules interact with the polar sites and diffuse in the network through a hopping mechanism with an approximate residence time in the order of tenths of nanoseconds per site [68], but the presence of localized free volume allows water molecules to agglomerate which influences its mobility. A comparative analysis of the diffusion coefficient ($D$) of the water molecules can help us understand the role of damage in the transport phenomenon of absorbed moisture. For atomistic simulations, $D$ can be calculated from the slope of the mean square displacement (MSD) curve and its details have been included in the SI.

Fig. 9 shows the MSD of water molecules over time for the 2 Å debond model. Similar plots for the other two damaged models have been included in Figure S8 of the SI and they have comparable trends. The MSD in the undamaged system has been included as a reference and we can observe that the water molecules have a much greater displacement which would eventually lead to a higher diffusion coefficient when a larger proportion of moisture is dispersed in the network. This is demonstrated by the flattening of the MSD curves as we move from the undamaged reference to a damaged system where the moisture is initially dispersed in the bulk, and finally to the damaged system which has the absorbed moisture concentrated at the interface. The visual flattening is confirmed by the diffusion coefficients as seen in Fig. 10. The x-axis in the plot shows the debond width and we have assumed that the undamaged reference has no measurable debonding between the fiber and the matrix (debond width of 0 Å). The diffusion coefficient (slope) was calculated in the common linear region between 500 ps and 2500 ps of the simulation trajectory and every scatter point in the plot is an average calculated from 3 representative models with the error bars signifying the standard deviation. The results show that as the damage increases in the system, the water molecules show decreased diffusivity owing to its accumulation near the damage site. It is interesting to point out that the movement of the water molecules is also impeded due to type-II polar interactions with the polymer network, but the diffusivity results in this study suggest that localized confinement near the damage site has a greater impact on moisture diffusion than secondary H-bonding interactions. We have already observed in Section 3.1 that the final moisture concentration near the damage site is directly proportional to the debond width. When the damage increases, greater clustering is observed at the interface even if the water molecules are dispersed in the composite matrix. This phenomenon is corroborated by

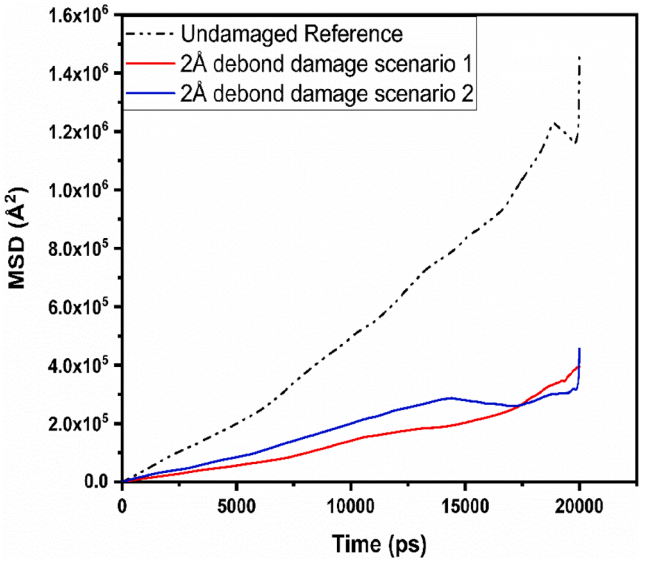


**Fig. 9.** MSD of the water molecules in the two damage scenarios for the 2 Å debond model.

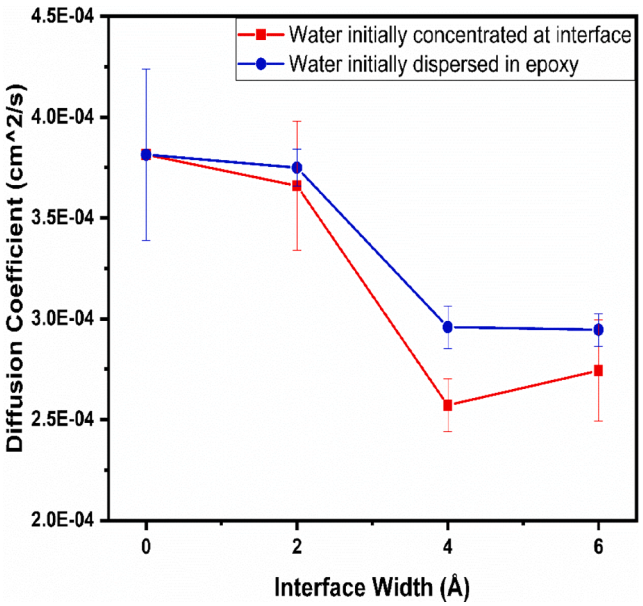


**Fig. 10.** Average diffusivity for the absorbed moisture as a function of interfacial width of fiber–matrix debond.

the diffusion coefficient as it decreases with increase in debond width. The initial concentration of the absorbed moisture also plays a role in the diffusivity. In damage scenario 1, all the water molecules are spatially confined together near the debond in the beginning of the simulation. Consequently, they diffuse out into the matrix slower when compared to scenario 2 where the water molecules are initially dispersed in the polymer network.

## 4. Conclusion

This simulation study helps us obtain a molecular understanding of the behavior of absorbed moisture in a damaged composite. The polymer-water interactions in a composite matrix is a widely studied research area and multiple studies have hypothesized the influence of different factors contributing to property degradation. The results in this study suggest that water molecules tend to cluster near the damage site regardless of the initial distribution of moisture in the damaged system. The non-bonded interactions are also influenced by damage as seen in the H-bonding activity of the water molecules. The increase in Type-I bonding with the introduction of damage reaffirms the theory that water molecules have a higher tendency to accumulate at the damage interface. We also observe that the interfacial energy at the fiber-matrix interface changes with the extent of damage which determines how quickly water starts migrating towards the damage interface. The combination of all of these molecular phenomena leads to spatial confinement of the absorbed water molecules near the interfacial debond and a hindered diffusion rate out into the polymer matrix as the damage area increases in the composite. These confined water molecules at the damage site will behave like free water in terms of its dielectric activity.

The results from this study are critical in understanding how moisture is absorbed in a polymer composite and how the difference in polymer-water interactions can help us in detecting damage in a composite. The ubiquitous presence of atmospheric moisture coupled with the inevitability of low energy impact events for an in-service composite guarantees absorption and based on this study we can conclude that the absorbed water molecules will tend to diffuse towards the damaged areas and exist as clusters of free water. This molecular level finding corroborates previous experimental studies, which have shown a localized rise in permittivity near barely visible damage sites in polymer-

based composites. These studies also show that the rise in permittivity is directly proportional to the extent of damage. Since clusters of water molecules exhibit bulk behavior, they have a much higher dielectric constant compared to polymer bound water molecules. In this study, a higher number of water molecules agglomerate at the damage site as the interface width increases. This indicates that a greater number of water molecules near the damage site will behave like 'free' water leading to a higher rise in localized permittivity which can be leveraged for both damage detection and quantification.

## Data availability

Data will be made available upon request.

### *CRediT authorship contribution statement*

**Rishabh D. Guha:** Conceptualization, Methodology, Software, Data curation, Visualization, Writing – original draft. **Farzin Rahmani:** Software, Investigation, Writing – review & editing. **Katherine Berkowitz:** Writing – review & editing. **Melissa Pasquinelli:** Software, Resources, Supervision. **Landon R. Grace:** Project administration, Funding acquisition, Supervision, Writing – review & editing.

## Declaration of Competing Interest

The authors declare that they have no known competing financial interests or personal relationships that could have appeared to influence the work reported in this paper.

### *Acknowledgements*

The authors would like to acknowledge the insight of Dr. Andrew Petersen (Data Sciences Research Specialist at NCSU) and the HPC cluster at NCSU for allotting us the computational time for running our simulations.

### *Funding sources*

This material is based upon work partially supported by the National Science Foundation under Grant No. CMMI-175482.

## Appendix A. Supplementary data

Supplementary data to this article can be found online at https://doi.org/10.1016/j.commatsci.2022.111690.

## References

[1] L. Garden, R.A. Pethrick, A dielectric study of water uptake in epoxy resin systems, J. Appl. Polym. Sci. 134 (2017).
[2] X. Chen, L. Yuan, Z. Zhang, et al., New glass fiber/bismaleimide composites with significantly improved flame retardancy, higher mechanical strength and lower dielectric loss, Compos. Part B: Eng. 71 (2015) 96–102.
[3] Z. Zhang, L. Yuan, G. Liang, et al., Fabrication and origin of flame retarding glass fiber/bismaleimide resin composites with high thermal stability, good mechanical properties, and a low dielectric constant and loss for high frequency copper clad laminates, RSC Adv. 6 (2016) 19638–19646.
[4] B. Dębska, L. Lichołai, Resin composites with high chemical resistance for application in civil engineering, Periodica Polytechnica Civ. Eng. 60 (2016) 281–287.
[5] L.R. Grace, The effect of moisture contamination on the relative permittivity of polymeric composite radar-protecting structures at X-band, Compos. Struct. 128 (2015) 305–312.
[6] F. Ellyin, C. Rohrbacher, The Influence of Aqueous Environment, Temperature and Cyclic Loading on Glass-Fibre/Epoxy Composite Laminates, J. Reinforced Plastics Compos. 22 (2003) 615–636.
[7] L. Kumosa, B. Benedikt, D. Armentrout, et al., Moisture absorption properties of unidirectional glass/polymer composites used in composite (non-ceramic) insulators, Compos. Part A: Appl. Sci. Manuf. 35 (2004) 1049–1063.
[8] A. Katunin, A. Wronkowicz-Katunin, D. Wachla, Impact damage assessment in polymer matrix composites using self-heating based vibrothermography, Compos. Struct. 214 (2019) 214–226.
[9] T. Skinner, S. Datta, A. Chattopadhyay, et al., Fatigue damage behavior in carbon fiber polymer composites under biaxial loading, Compos. Part B: Eng. 174 (2019), 106942.
[10] W. Li, C. Xu, Y. Cho, Characterization of degradation progressive in composite laminates subjected to thermal fatigue and moisture diffusion by lamb waves, Sensors 16 (2016) 260.
[11] K. Berkowitz, O. Idolor, M. Pankow, et al., Combined effects of impact damage and moisture exposure on composite radome dielectric properties. in: SAMPE Long Beach 2018 Conference and Exhibition. Soc. for the Advancement of Material and Process Engineering, 2018.
[12] T.S. Ellis, F.E. Karasz, Interaction of epoxy resins with water: the depression of glass transition temperature, Polymer 25 (5) (1984) 664–669.
[13] M.T. Stoffels, M.P. Staiger, C.M. Bishop, Reduced interfacial adhesion in glass fibre-epoxy composites due to water absorption via molecular dynamics simulations, Compos. Part A: Appl. Sci. Manuf. 118 (2019) 99–105.
[14] P.S. Theocaris, E.A. Kontou, G.C. Papanicolaou, The effect of moisture absorption on the thermomechanical properties of particulates, Colloid Polym. Sci. 261 (5) (1983) 394–403.
[15] S.K. Gupta, M. Hojjati, Microcrack Detection in Composite Laminates at Early Stage of Thermal Cycling Using Moisture/Freeze/Dry Cycle, Int. J. Compos. Mater. 9 (2019) 7–15.
[16] P. Duchene, S. Chaki, A. Ayadi, P. Krawczak, A review of non-destructive techniques used for mechanical damage assessment in polymer composites, J. Mater. Sci. 53 (11) (2018) 7915–7938.
[17] R.H. Bossi, V. Giurgiutiu, Nondestructive testing of damage in aerospace composite, in: Polymer Composites in the Aerospace Industry. Anonymous, Elsevier, 2015, pp. 413-448.
[18] M.R. Jolly, A. Prabhakar, B. Sturzu, K. Hollstein, R. Singh, S. Thomas, P. Foote, A. Shaw, Review of non-destructive testing (NDT) techniques and their applicability to thick walled composites, Procedia CIRP 38 (2015) 129–136.
[19] K. Berkowitz, R.d. Guha, O. Idolor, et al., Impact Damage Detection Limits of Microwave NDE Technique for Polymer Composites. in: Proceedings of the American Society for Composites—Thirty-Sixth Technical Conference on Composite Materials, 2021.
[20] O. Idolor, R., Guha, L. grace, A Dielectric Resonant Cavity Method for Monitoring of Damage Progression in Moisture-Contaminated Composites. in: Proceedings of the American Society for Composites—Thirty-Third Technical Conference, 2018.
[21] O. Idolor, R. Guha, L. Bilich, et al., 2-Dimensional Mapping of Damage in Moisture Contaminated Polymer Composites Using Dielectric Properties. Proceedings of the American Society for Composites—Thirty-Fourth Technical Conference, 2019.
[22] O. Idolor, R.D. Guha, K. Berkowitz, L. Grace, An experimental study of the dynamic molecular state of transient moisture in damaged polymer composites, Polymer Composites 42 (7) (2021) 3391–3403.
[23] IDOLOR, O., GUHA, R., BERKOWITZ, K., & GRACE, L. (2020, September). Damage Detection in Polymer Matrix Composites by Analysis of Polymer-Water Interactions Using Near-Infrared Spectroscopy. In *Proceedings of the American Society for Composites 35th Technical Conference*.
[24] O. Idolor, R.D. Guha, K. Berkowitz, C. Geiger, M. Davenport, L. Grace, Polymer-water interactions and damage detection in polymer matrix composites, Compos. Part B: Eng. 211 (2021) 108637.
[25] P. Moy, F.E. Karasz, Epoxy-water interactions, Polym. Eng. Sci. 20 (4) (1980) 315–319.
[26] A. Apicella, R. Tessieri, C. de Cataldis, Sorption modes of water in glassy epoxies, J. Membr. Sci. 18 (1984) 211–225.
[27] R.A. Pethrick, E.A. Hollins, I. McEwan, et al., Dielectric, Mechanical and Structural, and Water Absorption Properties of a Thermoplastic-Modified Epoxy Resin: Poly (ether sulfone)−Amine Cured Epoxy Resin, Macromolecules 29 (1996) 5208–5214.
[28] A. Herrera-Gómez, G. Velázquez-Cruz, M.O. Martín-Polo, Analysis of the water bound to a polymer matrix by infrared spectroscopy, J. Appl. Phys. 89 (10) (2001) 5431–5437.
[29] P. Musto, G. Ragosta, L. Mascia, Vibrational Spectroscopy Evidence for the Dual Nature of Water Sorbed into Epoxy Resins, Chem. Mater. 12 (5) (2000) 1331–1341.
[30] P. Musto, L. Mascia, G. Ragosta, G. Scarinzi, P. Villano, The transport of water in a tetrafunctional epoxy resin by near-infrared Fourier transform spectroscopy, Polymer 41 (2) (2000) 565–574.
[31] P. Musto, G. Ragosta, G. Scarinzi, et al., Probing the molecular interactions in the diffusion of water through epoxy and epoxy–bismaleimide networks, J. Polym. Sci. Part B: Polym. Phys. 40 (2002) 922–938.
[32] L.R. Grace, M.C. Altan, Characterization of anisotropic moisture absorption in polymeric composites using hindered diffusion model, Compos. Part A: Appl. Sci. Manuf. 43 (2012) 1187–1196.
[33] L.R. Grace, M.C. Altan, Non-fickian three-dimensional hindered moisture absorption in polymeric composites: Model development and validation, Polymer Composites 34 (2013) 1144–1157.
[34] L.R. Grace, M.C. Altan, Three-dimensional anisotropic moisture absorption in quartz-reinforced bismaleimide laminates, Polym. Eng. Sci. 54 (2014) 137–146.
[35] A.P. Tran, M.R.M. Ardekani, S. Lambot, Coupling of dielectric mixing models with full-wave ground-penetrating radar signal inversion for sandy-soil-moisture estimation, Geophysics 77 (2012) H33–H44.
[36] D.P. Fernandez, Y. Mulev, A. Goodwin, et al., A database for the static dielectric constant of water and steam, J. Phys. Chem. Reference Data 24 (1995) 33–70.
[37] I. Yarovsky, E. Evans, Computer simulation of structure and properties of crosslinked polymers: application to epoxy resins, Polymer 43 (2002) 963–969.

[38] V. Varshney, S.S. Patnaik, A.K. Roy, et al., A Molecular Dynamics Study of Epoxy-Based Networks: Cross-Linking Procedure and Prediction of Molecular and Material Properties, Macromolecules 41 (2008) 6837–6842.
[39] C. Li, A. Strachan, Molecular simulations of crosslinking process of thermosetting polymers, Polymer 51 (2010) 6058–6070.
[40] J. Mijović, H. Zhang, Molecular Dynamics Simulation Study of Motions and Interactions of Water in a Polymer Network, J. Phys. Chem. B 108 (2004) 2557–2563.
[41] S. Masoumi, H. Valipour, Effects of moisture exposure on the crosslinked epoxy system: an atomistic study, Model. Simulation Mater. Sci. Eng. 24 (3) (2016) 035011.
[42] L.-h. Tam, D. Lau, C. Wu, Understanding interaction and dynamics of water molecules in the epoxy via molecular dynamics simulation, Molecular Simulation 45 (2) (2019) 120–128.
[43] R.D. Guha, O. Idolor, L. Grace, Molecular Dynamics (MD) Simulation of a Polymer Composite Matrix with Varying Degree of Moisture: Investigation of Secondary Bonding Interactions. in: Proceedings of the American Society for Composites—Thirty-Fourth Technical Conference, 2019.
[44] R.D. Guha, O. Idolor, L. Grace, An atomistic simulation study investigating the effect of varying network structure and polarity in a moisture contaminated epoxy network, Computational Mater. Sci. 179 (2020) 109683.
[45] R.D. Guha, O. Idolor, K. Berkowitz, M. Pasquinelli, L.R. Grace, Exploring secondary interactions and the role of temperature in moisture-contaminated polymer networks through molecular simulations, Soft Matter. 17 (10) (2021) 2942–2956.
[46] Y.C. Lin, X. Chen, Investigation of moisture diffusion in epoxy system: Experiments and molecular dynamics simulations, Chem. Phys. Lett. 412 (2005) 322–326.
[47] W. Li, L. Zhang, M. Zhang, et al., The effects of interfacial water and SiO2 surface wettability on the adhesion properties of SiO2 in epoxy nanocomposites, Appl. Surf. Sci. 502 (2020), 144151.
[48] Y. Hu, W. Ji, L. Zhang, Water-induced damage revolution of the carbon nanotube reinforced poly (methyl methacrylate) composites, Compos. Part A: Appl. Sci. Manuf. 136 (2020), 105954.
[49] L. Tam, C.L. Chow, D. Lau, Moisture effect on interfacial integrity of epoxy-bonded system: a hierarchical approach, Nanotechnology 29 (2017), 024001.
[50] L. Tam, L. He, C. Wu, Molecular dynamics study on the effect of salt environment on interfacial structure, stress, and adhesion of carbon fiber/epoxy interface, Composite Interfaces 26 (2019) 431–447.
[51] L. Tam, A. Zhou, C. Wu, Nanomechanical behavior of carbon fiber/epoxy interface in hygrothermal conditioning: A molecular dynamics study, Mater. Today Commun. 19 (2019) 495–505.
[52] O. Büyüköztürk, M.J. Buehler, D. Lau, C. Tuakta, Structural solution using molecular dynamics: Fundamentals and a case study of epoxy-silica interface, Int. J. Solids Struct. 48 (14-15) (2011) 2131–2140.
[53] F. Vuković, T.R. Walsh, Moisture Ingress at the Molecular Scale in Hygrothermal Aging of Fiber-Epoxy Interfaces, ACS Appl. Mater. Interfaces 12 (49) (2020) 55278–55289.
[54] LAMMPS: Large-scale Atomic/Molecular Massively Parallel Simulator (https://lammps.sandia.gov/index.html).
[55] P. Santak, G. Conduit, Enhancing NEMD with automatic shear rate sampling to model viscosity and correction of systematic errors in modeling density: Application to linear and light branched alkanes, J. Chem. Phys. 153 (1) (2020) 014102.
[56] P. Prathumrat, I. Sbarski, E. Hajizadeh, et al., A comparative study of force fields for predicting shape memory properties of liquid crystalline elastomers using molecular dynamic simulations, J. Appl. Phys. 129 (2021), 155101.
[57] J. Kuntail, S. Pal, I. Sinha, Interfacial phenomena during Fenton reaction on starch stabilized magnetite nanoparticles: Molecular dynamics and experimental investigations, J. Molecular Liquids 318 (2020), 114037.
[58] M. Deng, V. Tan, T.E. Tay, Atomistic modeling: interfacial diffusion and adhesion of polycarbonate and silanes, Polymer 45 (2004) 6399–6407.
[59] M. Zhang, B. Jiang, C. Chen, et al., The effect of temperature and strain rate on the interfacial behavior of glass fiber reinforced polypropylene composites: a molecular dynamics study, Polymers 11 (2019) 1766.
[60] S. Yu, S. Yang, M. Cho, Multi-scale modeling of cross-linked epoxy nanocomposites, Polymer 50 (2009) 945–952.
[61] B. Li, J. Chen, Y. Lv, et al., Influence of Humidity on Fatigue Performance of CFRP: A Molecular Simulation, Polymers 13 (2021) 140.
[62] S. Kwon, M.Y. Lee, S. Yang, Molecular dynamics approach on the hygroelastic behavior of epoxy/graphene nanocomposites, J. Mech. Sci. Technol. 33 (2019) 741–747.
[63] J. Liu, Z. Liu, S. Yuan, et al., Synthesis, crystal structures, and spectral characterization of tetranuclear Mn (II) complex with a new Schiff base ligand and molecular dynamics studies on inhibition properties of such Schiff base, J. Mol. Struct. 1037 (2013) 191–199.
[64] J. Zeng, J. Zhang, X. Gong, Molecular dynamics simulation of interaction between benzotriazoles and cuprous oxide crystal, Computat. Theoretical Chem. 963 (2011) 110–114.
[65] A.D. Wade, L. Wang, D.J. Huggins, Assimilating Radial Distribution Functions To Build Water Models with Improved Structural Properties, J. Chem. Inform. Model. 58 (2018) 1766–1778.
[66] R.E. Skyner, J.B. Mitchell, C.R. Groom, Probing the average distribution of water in organic hydrate crystal structures with radial distribution functions (RDFs), CrystEngComm. 19 (2017) 641–652.
[67] A.G. Airale, M. Carello, A. Ferraris et al. 2016. Moisture effect on mechanical properties of polymeric composite materials, in: AIP Conference Proceedings, vol. 1736: 020020. AIP Publishing LLC.
[68] L.W. Jelinski, J.J. Dumais, A.L. Cholli, et al., Nature of the water-epoxy interaction, Macromolecules 18 (1985) 1091–1095.